Graphical Abstract

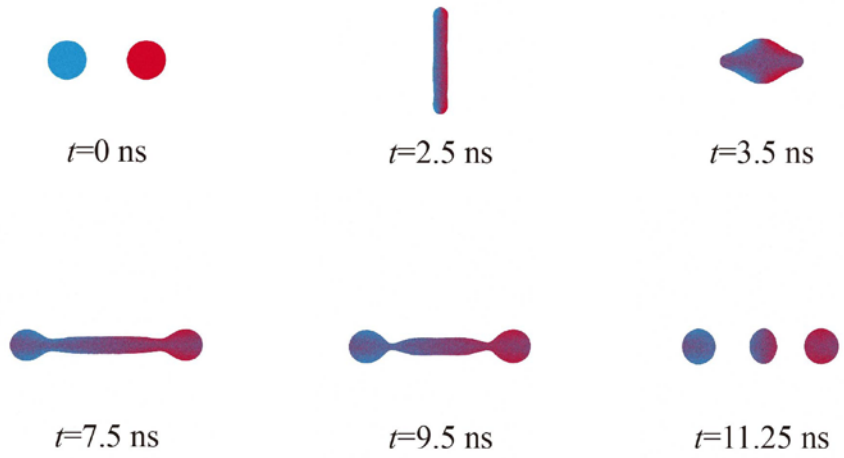

Reflexive Separation Regime in Nanoscale Droplet Collision

Size Effects on Dynamics of Nanodroplets in Binary Head-on Collisions

Yi Ran Zhang[1,2], Zijian Zhao[3,4], Kai H. Luo[5,*] and Baolu Shi[6]

[1] *Center for Combustion Energy, Department of Energy and Power Engineering, Key Laboratory for Thermal Science and Power Engineering of Ministry of Education, Tsinghua University, Beijing 100084, China*

[2] *China Electric Power Planning & Engineering Institute, Beijing 100120, China*

[3] *Global Energy Interconnection Development and Cooperation Organization, Beijing 100031, China*

[4] *Department of Earth System Science, Tsinghua University, Beijing 100084, China*

[5] *Department of Mechanical Engineering, University College London, Torrington Place, London WC1E 7JE, United Kingdom*

[6] *School of Aerospace Engineering, Beijing Institute of Technology, No. 5 ZhongGuanCun South Street, Haidian, Beijing 100081, China*

***** Corresponding Author: Kai H. Luo (Prof. K. H. Luo)

Email: K.Luo@ucl.ac.uk

Postal Address: Department of Mechanical Engineering, University College London, Torrington Place, London WC1E 7JE, UK

Fax: +44 (0)20 7388 0180

Abstract

Head-on collision dynamics of 10, 50 and 100 nm droplets are investigated in vacuum by molecular dynamics, involving 35,858, 4,506,410 and 36,051,466 molecules, respectively. A variety of droplet collision dynamics are observed, such as coalescence, hole formation and shattering, as a function of the Weber number. It is found for the first time that the collision and reflexive separation can occur in the nanodroplet regime when the droplet diameter reaches 100 nm but not for 10 or 50 nm droplets. The size effect in droplet collisions is studied based on the analysis of stretching factors, energy dissipation and collision outcomes for droplets of different diameters. The kinetic energy dissipation due to the atomic interactions at nanoscales is identified to significantly influence the occurrence or otherwise of reflexive separation. Through quantitative analysis of the evolution of the internal structure of the 100 nm nanodroplets collision at the Weber number of 277, it is revealed for the first time that molecules from both parent nanodroplets have penetrated the full length of the merged nanodroplet in the direction of collision, due to a combination of molecular mixing and internal currents. Consequently, all three child nanodroplets have molecules from both parent nanodroplets, contrary to the perception gained from common imaging techniques. The results show that the dynamics, outcomes and mechanisms of nanodroplet collisions have both similarities and differences compared with their micro- and macro-counterparts.

Keywords: Reflexive separation; Droplet collision; Nanoscale; Size effect; Molecular

dynamics

Highlights:

- Discovery of a collision and reflexive separation regime in nanodroplet collisions for the first time
- Identification of the size effect on droplet collision outcomes and mechanisms behind, from an atomic perspective
- Identification and quantification of internal molecular movement in both parent and child nanodroplets in the collision and reflexive separation regime for the first time

1. Introduction

Droplet collisions are a frequent and important phenomenon in industry and nature[1–4], for instance, in nuclear reactors[5] and in the process of spraying[6,7] such as plasma spray[8] and high pressure spray cleaning[9,10]. A rich variety of collision phenomena have been recorded by experiments [11]. Numerical simulations[12-16] have also been employed to reproduce some phenomena and provide additional insight. In numerical simulation and experimental studies, droplet radius ranged from 10nm to 150μm. Experiments[11] have identified coalescence, bounce, reflexive separation and shattering regimes for head-on hydrocarbon droplet collisions with increasing Webber number. Qian and Law[17] identified the existence of a bounce regime in water droplet collisions and determined the key parameters at low collision energy. Pan et al.[18] analyzed instability of the droplet's rim in detail in the shattering regime with the Weber number up to 5000. Zhang and Law[19] conducted a comprehensive theoretical analysis for head-on binary droplet collisions in two dimensions. Li's numerical model achieved a reasonable agreement with experimental results by solving the Navier-Stokes equations on a moving adaptive mesh[20]. However, experiments or macroscopic numerical methods had difficulty obtaining collision details, especially those at the interfaces where important physics occur at atomic scales[21,22]. Recently, we have found that nanoscale droplets show different collision behaviors from macroscale or microscale droplets using molecular dynamics (MD). Using the MD approach, we have successfully reproduced the bounce regime in nanoscale droplet collision for the first time[24]. Such a phenomenon has only been observed in microdroplets experiments[1]. At

high impact numbers, we have also observed a new hole regime which went beyond previous understanding of droplet collisions[23]. Previous numerical studies failed to observe these regimes because they were not able to resolve the interfacial zone as it reached mean molecular free path, and artificial rupture of the thin film is required to mimic droplets coalescence/separation[13]. Until now, the reflexive separation regime in the collision of nanodroplets has never been reproduced even by MD. At nanoscales, size effect is likely to play a more important role than at micro- and macroscales. Due to the huge computational cost, previous MD studies mainly focus on water and argon droplets with simple interatomic potential, and droplet diameters under 20 nm[25]. To better understand nanoscale droplet collisions and to build a bridge between nano-, micro- and macrodroplets, droplets of different sizes reaching larger diameters need to be investigated[26]. Our current understanding of nanoscale droplet collisions is still very limited, and the validity of the current macroscale models for predicting the transition Weber number from coalescence to reflexive separation is worth checking at nanoscales.

In this research, we conduct a comprehensive study on nanodroplets collision dynamics using state of the art MD. Section 2 introduces the molecular dynamics methodology and initial simulation setup. Section 3.1 discusses different collision outcomes. Section 3.2 analyzes mixing and mass transfer in reflexive separation. Section 3.3 illustrates the size effect in droplet collisions. The conclusions of the research are drawn in Section 4.

2. Molecular dynamics simulations

In MD simulations, the Newtonian equations of motion are solved for individual atoms and molecules subjected to intermolecular forces. For a system with atoms coordinates X and atoms velocities V, the Newtonian equations can be written as follows:

$$M\dot{V}(t) = -\nabla U(X) = F(X) \tag{1}$$

$$V(t) = \dot{X}(t) \tag{2}$$

where $U(X)$ and M represent the energy potential function and mass, respectively. From the negative gradient of $U(X)$, we can obtain the force F acting on each atom. Given the initial positions and velocities, subsequent positions and velocities can be obtained. MD simulations have been employed in different research fields like multiphase flow, materials science and biochemistry[24,27]. Due to their high computational costs, existing MD simulations are typically restricted to an atom or molecule number on the order of 10^6 and a simulation time of nanoseconds. For computational efficiency and physical clarity, periodic boundary conditions are usually employed, although open boundary conditions can also be deployed.

We investigated head-on binary droplet collisions, which is a canonical problem in droplet dynamics. The initial setup of the two nanodroplets simulation system is shown in Figure 1. The two droplets were initially placed in the cubic simulation box. The simulation system comprises 35,858, 4,506,410 and 36,051,466 molecules in total for the 10, 50 and 100 nm droplets, respectively. Droplet collision occurs in the x-axis

direction. In previous studies[23], the maximum diameter of colliding water droplets in MD simulations was 10.6 nm. Being able to investigate collisions of up to 100 nm droplets in our studies is an important milestone in the research field using MD, which provides new insights.

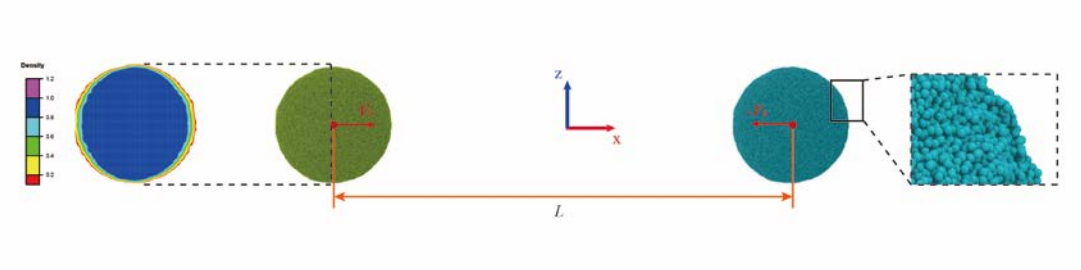

Figure 1. Configuration of the droplet collision system.

The mono-molecular mW water model has been adopted to describe the water molecules in molecular dynamics. The model is derived from the Stillinger-Weber multi-body potential and first proposed by Molinero and Moore[28]. It is a coarse-grained model and is able to accurately reproduce properties of liquid water. Full expressions of the mW water model are shown in Eqs. 3-5.

$$\mathrm{U} = \sum_{i}\sum_{j>1} \varphi_2(r_{ij}) + \sum_{i}\sum_{j\neq i}\sum_{k>j} \varphi_3(r_{ij}, r_{jk}, \theta_{ijk}) \tag{3}$$

$$\varphi_2(r) = A\varepsilon\left[B\left(\frac{\sigma_0}{r}\right)^p - \left(\frac{\sigma_0}{r}\right)^q\right] exp\left(\frac{\sigma_0}{r - a\sigma_0}\right) \tag{4}$$

$$\varphi_3(r, s, \theta) = \lambda\varepsilon[cos\theta - cos\theta_0]^2 exp\left(\frac{\gamma\sigma_0}{r - a\sigma_0}\right) exp\left(\frac{\gamma\sigma_0}{s - a\sigma_0}\right) \tag{5}$$

The total energy comprises two-body and three-body terms. In Eqs. (3), (4) and (5), φ_2 is the two-body term and φ_3 is the three-body term, r represents the inter-molecule distance, σ_0 is the distance where inter-particle potential is zero, ε represents the minimum energy. Subscripts i and j are molecule indexes in the system. Table 1

illustrates all the parameters selected in this research. Periodic boundary conditions were imposed and a 16 Å cut-off distance was applied.

Table 1. Values of potential parameters

σ_0	ε	a	λ	γ	$\cos\theta_0$	A	B	p	q
2.3925	6.189	1.8	23.15	1.2	-0.33	7.0496	0.6022	4.0	0.0

Droplet equilibration simulations were first conducted in vacuum. The canonical ensemble (NVT) was employed with a temperature of 300 K and a time step of 2 fs. After the initial equilibrium process, two droplets that are going to collide were placed in the centre of a cubic simulation box and a further equilibrium simulation was conducted. Collision simulations were conducted in micro-canonical ensemble (NVE) after all equilibrium simulations with initial temperature of 300 K. In vacuum, molecules in the environment only comprise water molecules evaporated from the droplets. Impact velocities with equal magnitude but opposite directions were assigned to the colliding droplets.

For the mW water model, viscosity and density are 851 μPas and 997 kg/m^3 in the simulations. We use the LAMMPS platform to perform molecular dynamics simulations[29]. Dynamic trajectories of atoms and molecules were displayed by Visual Molecular Dynamics (VMD)[30] and OVITO[31].

3. Results and Discussion

3.1. Reflexive separation regime in nanoscale droplet collision

In macroscale droplet collisions, the impact kinetic energy converts to surface energy by forming a disk. After that, the disk contracts and forms a cylinder. A

dumbbell is formed because of outwardly axial internal motion. The reflexive separation occurs as a balance of surface tension and outward motion. The reflexive separation regime occurs when the outward motion is able to split the dumbbell. If the outward motion is not strong enough, the coalescence regime occurs. Dimensionless parameters like the Reynolds number and Weber number are used to describe droplet collisions[32–34]. The Weber number compares droplet's inertia with its surface tension and the Reynolds number compares droplet's inertial force to its viscous force. They are defined as follows:

$$We = \frac{2R\rho U^2}{\sigma} \tag{6}$$

$$Re = \frac{2RU}{\upsilon} \tag{7}$$

where U is the relative impact velocity, R represents the droplet radius, ρ is the droplet density, σ and υ represent the droplet surface tension and dynamic viscosity. In our investigation, the surface tension is 66 $\mathrm{mJm^2}$ and the Weber number ranges from 10 to 600.

The reflexive separation phenomenon has never been observed in nano-scale droplet collisions. Svanberg[26] concluded that reflexive separation occurs with a cluster diameter larger than 5 nm. For the 10 nm droplets as shown in Fig. 2, coalescence, hole formation and shattering regimes were observed. As the Weber number reached 277, the droplets first approached each other and formed a disk. After maximum spreading state, the disk then contracted and evolved into a cylinder instead of a dumbbell because the outwardly axial motion is not sufficient. The surface tension of the merged mass pulled the end of cylinder back and reflexive separation was not observed, which is

consistent with previous studies[17]. Due to viscous force, a large amount of initial kinetic energy dissipated. As a result, the residual outward internal motion is too weak to form a dumbbell. When the Weber number was increased to 426 and 540, respectively, the hole formation and shattering regimes were observed, as shown in the middle and bottom rows of Fig. 2. The reflexive separation regime was not observed for the 10 nm droplet collision.

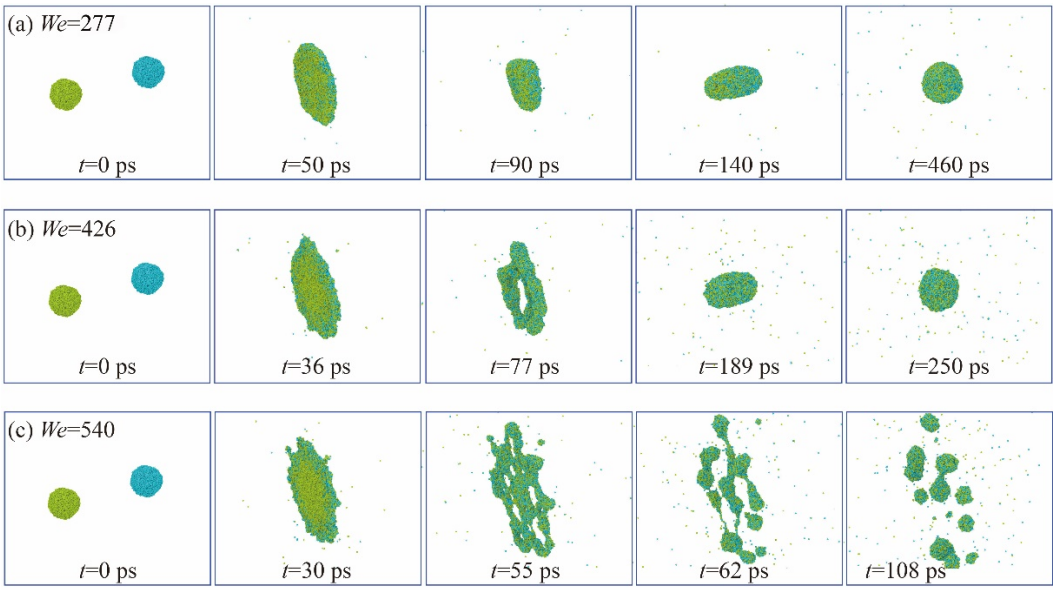

Figure 2. Snapshots of 10 nm droplet collisions at the Weber number of (a) 277, (b) 426 and (c) 540, respectively. The blue and yellow colours indicate molecules of different origins.

For the 50 nm droplet collision in Fig. 3, the formation of dumbbell can be observed while the reflexive separation regime is still absent. When the Weber number reached 277, the two droplets first approached each other and formed a dimpled disk. Through a kinetic energy evolution analysis in Fig. 4, at the maximum spreading state, the dimpled disk had the lowest kinetic energy (t = 0.65 ns). The kinetic energy in Fig. 4 is the total kinetic energy of all atoms in the system, which represents total kinetic

energy of the whole system. The disk then contracted and evolved into the dumbbell because of the outwardly axial internal motion. At the maximum stretching state (t = 1.15 ns), the merged mass contracted under the surface tension because the outwardly axial internal motion was not able to split the dumbell up. In the process of contracting, the ligament in the middle of the dumbbell became narrow and finally contracted to form a single droplet.

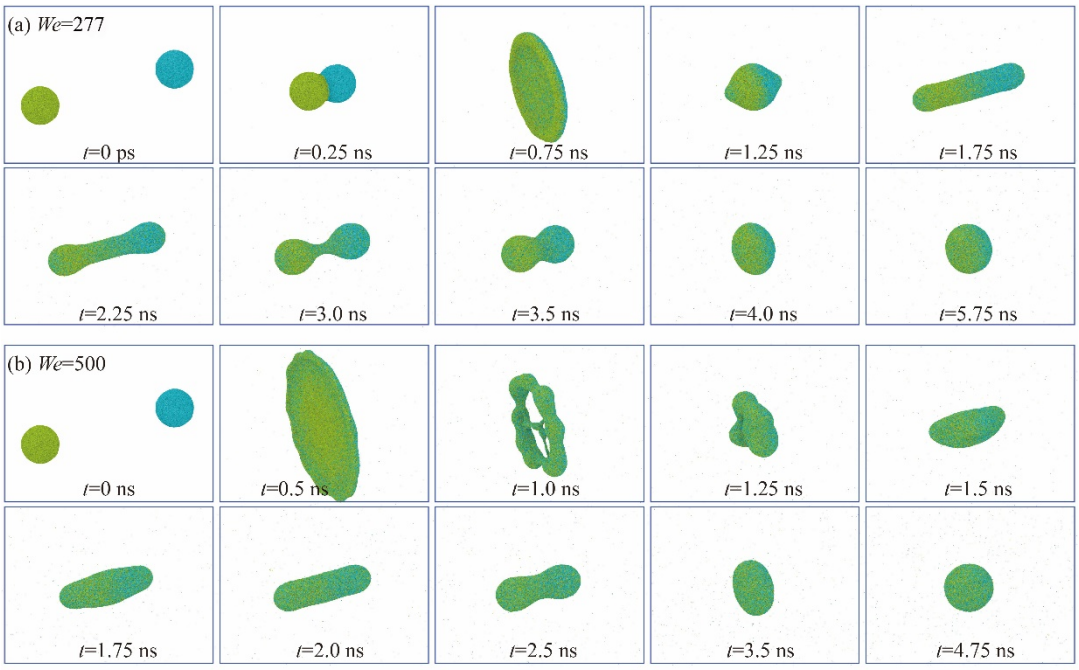

Figure 3. Snapshots of 50 nm droplet collisions at the Weber number of (a) 277 and (b) 500, respectively. The blue and yellow colours indicate molecules of different origins.

When the Weber number increased to 500, a higher initial kinetic energy was provided. Formation of holes was observed in the disk state (t = 1.0 ns), which has also been discovered in the 10 nm droplet collisions. Figure 4 compares kinetic energy evolutions for the Webber number at 277 and 500. By forming holes, kinetic energy

dissipated dramatically. As a result, the kinetic energy peak at the Weber number of 277 is sharper than that of 500. The kinetic energy at the first peak is 429,990 and 15,423 kJ/mol higher than the final stable droplet status at the Weber number of 277 and 500, respectively.

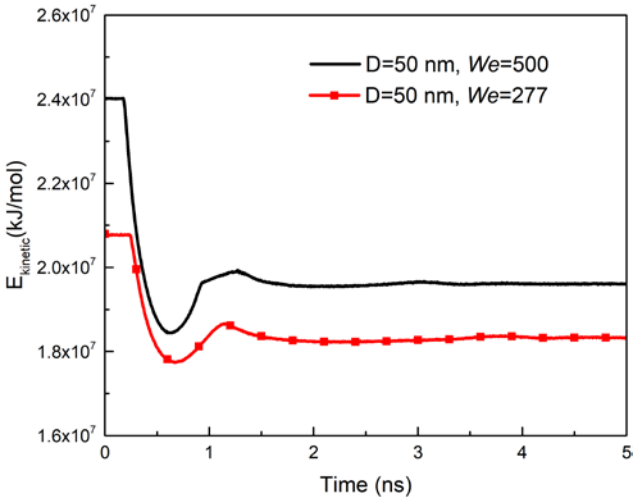

Figure 4. Kinetic energy evolutions of 50 nm droplet collisions at the Weber number of 277 and 500, respectively.

For the 100 nm droplet collisions, the reflexive separation regime was observed at the Weber number of 200. This is the first time that the reflexive separation regime is observed in nanodroplet collisions, which completes the regime map of nanodroplets collisions. As shown in Fig. 5, the reflexive separation includes four main stages. In the first stage (t<2.0 ns), the two droplets approached each other and formed a dimpled disk. The second stage (t=2.0~3.5 ns) started from the maximum spreading state, the disk contracted and evolved from a disk into a cylinder. In the third stage (t=3.5~5.5 ns), a dumbbell formed because of the outwardly axial momentum and thus outward internal motion. In the fourth stage (t=5.5~10.0 ns), the ligament (the bar between the bells) became narrower and narrower, unti it finally “pinched off” in the middle, with the

formation of two droplets under surface tension effects. Apparently, the two droplets at the final stage contain their original molecules, respectively, despite the collision and coalescence intermediate processes. This, however, could be misleading as the next case may reveal.

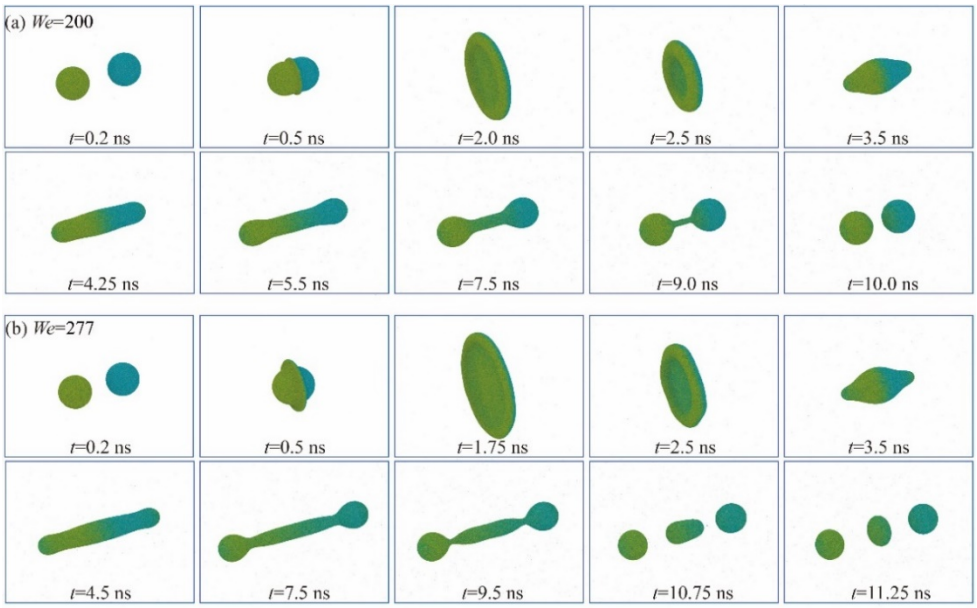

Figure 5. Snapshots of 100 nm droplet collisions at the Weber number of (a) 200 and (b) 277, respectively. The blue and yellow colours indicate molecules of different origins.

When the Weber number increased to 277, the collision process includes five main stages, with the initial stages similar to the Weber number 200 case. Due to the increased Weber number, however, the outward stretching momentum is higher and consequently the dumbbell has a much longer bar. “End-pinching” finally occurs at both ends, leaving a long liquid filament in between. This resembles the “end-pinching” mechanism in previous micro-droplet collision experiments[17]. In the fifth stage, the filament contracts to form a satellite droplet under the influence of surface tension. It is noted that molecular mixing takes place in the satellite droplet, which was not observed

before in experiments. On the surface, it appears that the left child droplet and the right child droplet contain purely molecules from the left parent droplet and the right parent droplet, respectively. Figure 6 compares the corresponding kinetic energy evolutions throughout the dynamic processes for the two Weber number cases. The key features are very similar between the two cases but there are quantitative differences.

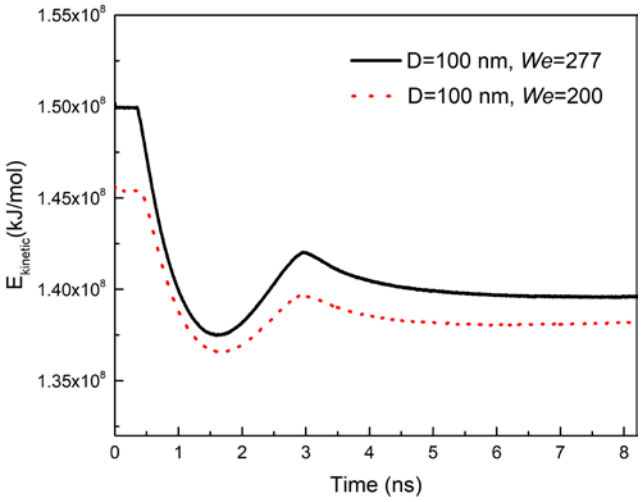

Figure 6. Kinetic energy evolutions of 100 nm droplet collisions at the Weber number of 200 and 277, respectively.

3.2. Mixing and mass transfer in the reflexive separation regime

Figure 7 demonstrates the reflexive separation for the 100 nm droplets at the Weber number of 277. To better illustrate how the droplets mix up at the molecular level, the cross-sectional view is provided and the two droplets are colored blue and red. Up to the stage of forming the disk of maximum diameter, there is little penetration of molecules from one droplet to the other (t = 1.75 ns). A clear boundary between the blue and the red zones can be observed in the merged disk, which indicates the mixing process did not occur. At t = 2.5 ns, mixing at the molecular level has taken place, with the formation of an diffusive interface. By the time t = 3.5 ns, a significant portion of

molecules have crossed the initial boundary between the two parent droplets, especially along the major horizontal axis and the minor vertical axis, due to a combination of molecular diffusion and, more importantly, internal currents. On the surface, however, a distinctive boundary between the blue and the red zones still exists, which creates a wrong impression that molecules never cross the interface as shown in Fig. 5. In the subsequent stages, the mixing process continued with the merged droplet stretched (t = 4.5 ns) and contracted (t = 9.5 ns). Finally, following the end-pinching, three child droplets were generated, with the left and the right droplets being of size and the middle satellite droplet having a smaller size.

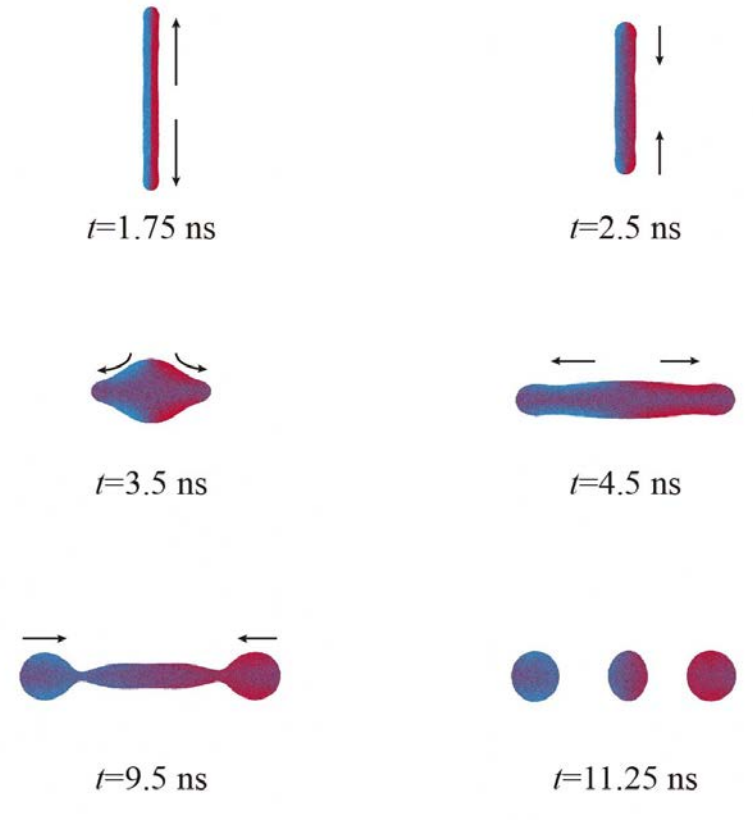

Figure 7. Cross-section view of reflexive separation regime (D=100 nm, *We*=277).

It is now clear that due to the the occurrence of mixing in the reflexive separation regime, the three child droplets contain molecules from both parent droplets. Figure 8

shows the composition analysis of the child and parent droplets. For the left child droplet, 74% and 26% of the molecules or mass of the left child droplet came from the left parent droplet and right droplet, respectively. The satellite droplet has an equal amount of each parent droplet. Symmetrically, 26% and 74% of the mass of the right child droplet came from the left parent droplet and the right parent droplet, respectively. From the left parent droplet, 54%, 28% and 18% of the molecules went to the left child droplet, satellite droplet and right child droplet, respectively, in the collision process. From the right parent droplet, the percentages were 18%, 28% and 54%, respectively.

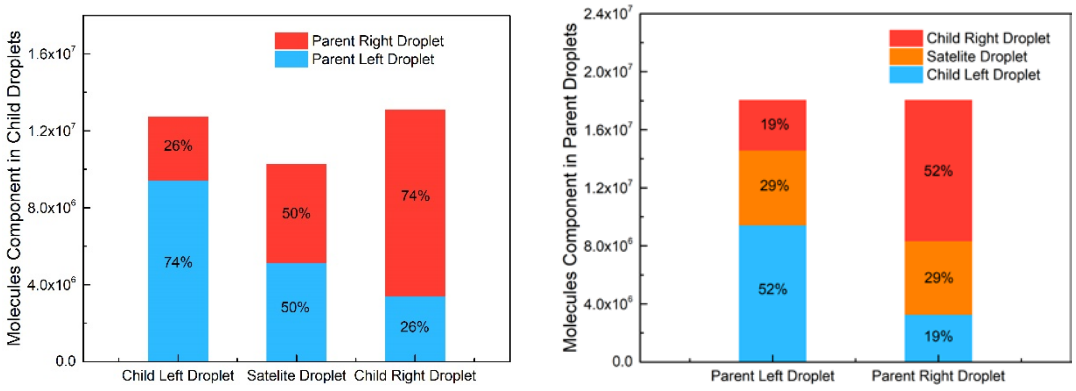

(a) (b)

Figure 8. Composition analysis of parent and child droplets in the reflexive separation regime (D=100 nm, *We*=277). (a) composition of child droplets in terms of molecules from parent droplets; (b) percentages of molecules from parent droplets donated to child droplets.

3.3. Size effect on droplet collision

From the above analysis, it is worth noting that the droplet diameter clearly affects the droplet collision outcomes. Gay[38] concluded that at the atomic level, there is a

transition from strong accommodation to weak accommodation. With increasing size, the effect of the interatomic forces diminishes.

3.3.1 Maximum stretching factor

The reflexive separation regime occurs when the maximum stretching factor of the droplet reaches a critical value. The maximum stretching factor is defined as follows,

$$\lambda_{max} = L_{max}/D_0 \tag{8}$$

where λ_{max} is the stretching factor at the maximum stretching state, L_{max} represents the maximum length at the maximum stretching state and D_0 is the droplet initial diameter. L_{max} and D_0 can be obtained from the density map on the cross section of the droplet collision, which is shown in Fig. 9. To obtain density contours, the simulation system is divided into grids and then the density is calculated by counting the number of atoms in each grid.

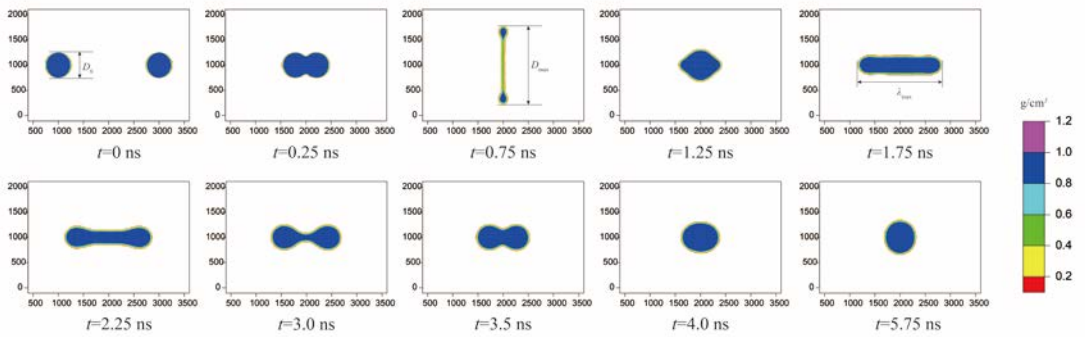

Figure 9. Density contours on the cross section of 50 nm droplet collisions at the Weber number of 277.

Figure 10 illustrates the maximum stretching factor for droplets with diameters of 10, 50 and 100 nm at different Weber numbers. For the 10 nm droplet, the stretching

factor rapidly increased to an almost constant value (around 1.61) with increasing Weber number. This implied that the initial kinetic energy dissipated quickly in the collision process. For the 50 nm droplet, the stretching factor increased to 4.4 at the Weber number of 358. The stretching factor then decreased with increasing Weber number, which could be attributed to a large amount of viscous dissipation during formation of holes. Therefore, the remaining kinetic energy of the outwardly axial internal motion was not sufficient to split the dumbbell apart and the merged mass finally contracted. For the 100 nm droplet, only collisions under the Weber number of 200 and 277 were conducted due to huge computational costs. The stretching factor reached 4.61 at the Weber number of 277 and the reflexive separation regime appeared. It is worth noting that at the same Weber number, the stretching factor for the 100 nm droplet is larger than those of 50 and 10 nm droplets.

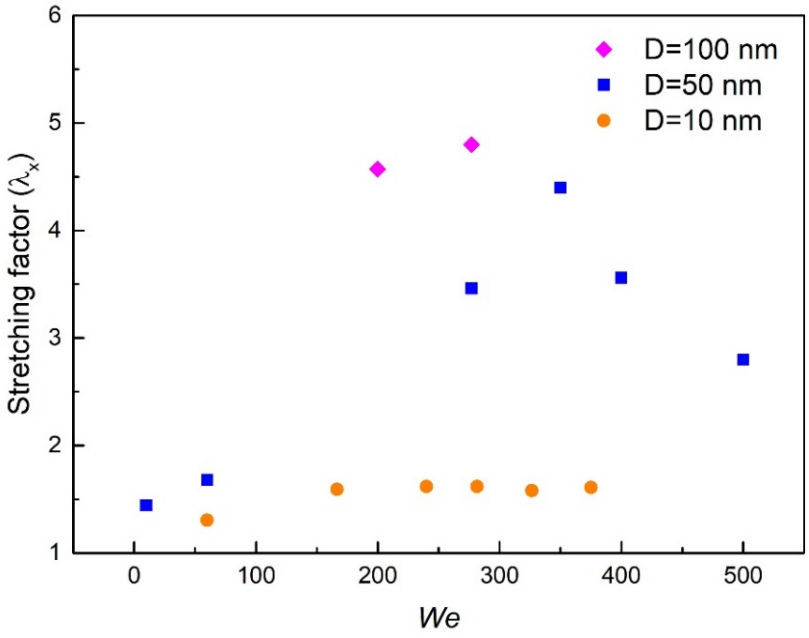

Figure 10. Maximum stretching factors of the 10, 50 and 100 nm droplets as a function of the Weber number.

3.3.2 Kinetic energy evolution

The kinetic energy evolutions at the Weber number of 277 for droplets with different diameters in the collision process are plotted in Fig. 11. The collision velocity is added at $t = 0$. As a result, the kinetic energy increases instantly.

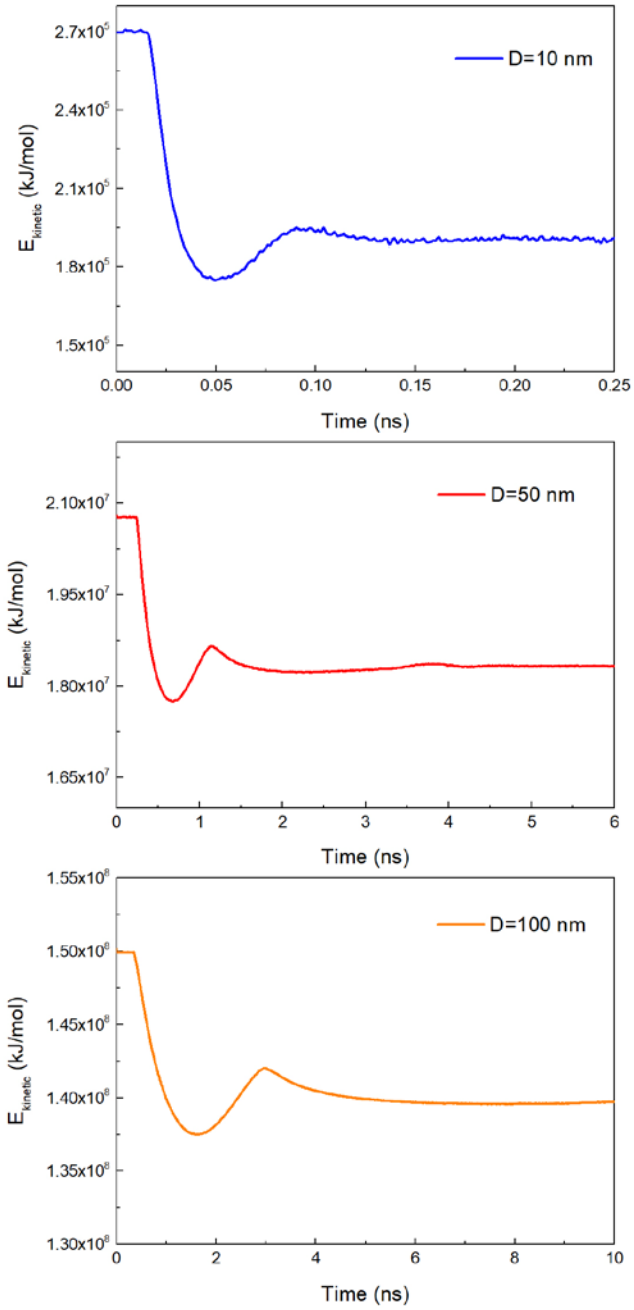

Figure 11. Kinetic energy evolutions for the 10, 50 and 100 nm droplets under the Weber number of 277.

As shown in Fig. 11, the kinetic energy peak decreases sharply with the decrease of droplet size. At the same impact Weber number, the smaller droplet takes shorter to dissipate the energy. The smaller the droplet, the smaller amount of the kinetic energy remains at the last point. The different energy evolutions explain the stretching factor differences in the collisions of the 10, 50 and 100 nm droplets at the same Weber number. In the third stage, the merged droplet moves away from the centre along the horizontal axis because of the outwardly axial internal motion. If the kinetic energy of the merged mass is sufficient, the reflexive separation phenomenon will occur.

3.3.3 Transition Weber number

Ashgriz and Poo first proposed a criterion to predict the transition Weber number from coalescence to reflexive separation regimes[2]. In their criterion, the viscous energy dissipation is neglected and the transition Weber number is around 19 for droplets with different viscosities. Qian and Law proposed another model which includes the viscous energy dissipation and is valid for low-viscosity droplets[17]:

$$We_c = \beta Oh + \gamma \tag{9}$$

$$Oh = \frac{\mu}{\sqrt{\rho\sigma L}} = \frac{\sqrt{We}}{Re} \tag{10}$$

where β is a geometry parameter, γ is an extra surface tension parameter and *Oh* is the Ohnesorge number. From Qian and Law's model, the transition Weber number of reflexive separation increases with the Ohnesorge number. Recently, Finotello et al. have extended the original model to viscous liquids[35]. The extended model for

coalescence to reflexive separation transition is:

$$We_c = \frac{12\Delta(1+\Delta^3)^2}{\Delta^6\eta_s + \eta_l} \cdot \frac{[(1.75-f)(1+\Delta^3)^{\frac{2}{3}} - (1-f)(1+\Delta^2)]}{1-f} \tag{11}$$

$$f = \frac{5Ca}{1+5Ca} \tag{12}$$

$$Ca = \frac{\mu U}{\sigma} \tag{13}$$

where η_s and η_l represent geometric factors, Δ is the size ratio, μ is the dynamic viscosity, *f* is an empirical fraction of effective kinetic energy fitted by direct numerical simulation (DNS) results. The Capillary number (Ca) measures relative effect of viscous force versus surface tension. This model clearly demonstrates the influence of surface tension and viscosity. Currently, this is the most accurate model in predicting the transition Weber number. Because the parameters are fitted by DNS results, the above findings are valid for macroscale droplet collisions. For example, for a 0.1 mm water droplet at the velocity of 9.6 m/s, the *Ca* number is 0.12 and the transition Weber number is 18.8.

Using the Finotello et al.'s model at nanoscales, the predicted transition Weber number is 2424, 1140 and 817 for the 10, 50 and 100 nm water droplets, respectively. However, the reflexive separation regime has never been observed in previous nanodroplets collision studies[36,37]. From our MD studies, the reflexive separation regime is absent in the collision of 10 and 50 nm droplets. For the 100 nm droplet, the reflexive separation regime occurs when the Weber number reaches 200, which is much lower than 817 predicted by Finotello et al.'s model. The discrepancy indicates that the size effect should be considered in droplet collisions. At nanoscales, due to the high

viscous dissipation, the current semi-empirical models that work well for macroscopic droplets do not accurately capture the dynamics of nanodroplets. To improve the current model, the parameter representing the fraction of effective kinetic energy should be refitted to nanoscale results. Due to computational resource limitations, our MD results are not yet extensive enough for refitting the model.

3.3.4 Comparison of droplet collision regimes at nanoscale and macroscale

Our investigation demonstrates that droplet size influences the outcomes of nanodroplet collisions. Individual interatomic collisions dominated collision force at nanoscales. As a result, the initial collision energy dissipated fast and the remaining kinetic energy is insufficient for the occurrence of reflexive separation below a certain droplet size. As the droplet approaches macroscales, collision force approaches inertia force level as the interatomic forces are submerged in the sum. Such a size effect explains that reflexive separation is more difficult to occur at nanoscale compared to macroscale.

Figure 12 demonstrates the different regimes of nanoscale and macroscale droplet collisions. For the water droplet with a diameter smaller than 50 nm, hole formation instead of reflexive separation occurs at intermediate Weber numbers. At the macroscale, reflexive separation instead of holes appears. Due to the size effect which could be attributed to the atom-atom interactions, there is a gradual transition from hole formation at nanoscales to reflexive separation at macroscales. Our investigation extends current understanding of droplet collisions, uncovering different dynamics and

outcomes of nanodroplet collisions as opposed to their micro- or macro-counterparts[18,39,40,41].

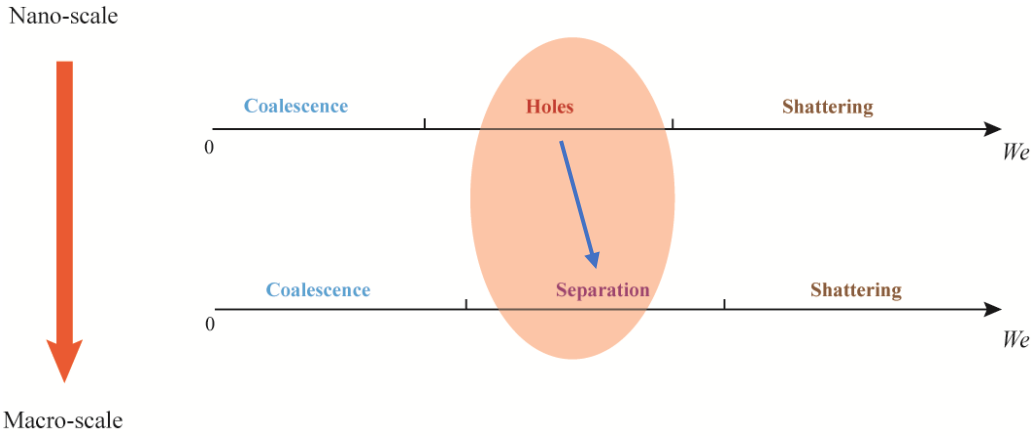

Figure 12. Comparison of droplet collision regimes at nanoscale and macroscale.

4. Conclusions

Through molecular dynamics simulations, we have investigated the size effect of nanodroplets collisions, with the droplet diameter ranging from 10 to 100 nm and the Weber number up to 540. We have uncovered the reflexive separation regime in the process of binary droplet collisions at nanoscale for the first time, which fills a knowledge gap in the relation between nanoscale and macroscale droplet collisions. A gradual transition from coalescence, hole formation and shattering regimes at nanoscales to coalescence, reflexive separation and shattering regimes has been observed for the first time in our investigation. End-pinching instead of shattering is found to be the main mechanism at nanoscales, resulting in the reflexive separation regime. Because interatomic interactions dominate at nanoscales, a large portion of the initial kinetic energy dissipated in collision. The energy dissipation makes reflexive separation difficult to occur at nanodroplets. An analysis of the kinetic energy evolution

in droplet collisions reveals that a larger droplet has a larger stretching factor. Additionally, the transition Weber number of reflexive separation predicted by previous macroscale models is not valid at nanoscales. This is attributed to the importance of viscous dissipation at nanoscales. A parameter representing the fraction of effective kinetic energy should be refitted to extensive results of nanodroplets collisions, which will be pursued in our follow-on research. Through quantitative analysis of the evolution of the internal structure of the 100 nm nanodroplets collision with the Weber number of 277, we reveal for the first time that molecules from both parent nanodroplets have penetrated the full length of the merged nanodroplet in the direction of collision, due to a combination of molecular mixing and internal currents. As a result, all three child nanodroplets have molecules from both parent nanodroplets, contrary to the perception gained from common imaging techniques. The present study provides atomic level insight into the dynamics, outcomes and the corresponding mechanisms of nanodroplets collisions, which have some similarities and some differences compared with their micro- and macro-counterparts.

Acknowledgments

Computations were performed partly on the Tsinghua High-Performance Parallel Computer and the UK national high-end computing service ARCHER. Support from the EPSRC project “UK Consortium on Mesoscale Engineering Sciences” under Grant Nos. EP/R029598/1 and EP/P022243/1 is acknowledged.

References

(1) J. R. Adam, N. R. Lindblad, and C. D. Hendricks, "The Collision, Coalescence, and Disruption of Water Droplets," J. Appl. Phys. **39**, 5173–5180 (1968).

(2) N. Ashgriz and J. Y. Poo, "Coalescence and Separation in Binary Collisions of Liquid Drops," J. Fluid Mech. **221**, 183 (1990).

(3) D. Liu, P. Zhang, C. K. Law, and Y. Guo, "Collision Dynamics and Mixing of Unequal-Size Droplets," Int. J. Heat Mass Transf. **57**, 421–428 (2013).

(4) G. M. Faeth, "Current Status of Droplet and Liquid Combustion," Prog. Energy Combust. Sci. **3**, 191–224 (1977).

(5) C. Focke, M. Kuschel, M. Sommerfeld, and D. Bothe, "Collision between High and Low Viscosity Droplets: Direct Numerical Simulations and Experiments," Int. J. Multiph. Flow **56**, 81–92 (2013).

(6) T. Hawa and M. R. Zachariah, "Coalescence Kinetics of Unequal Sized Nanoparticles," Aerosol Sci. **37**, 1–15 (2006).

(7) Q. Li, K. H. Luo, Q. J. Kang, Y. L. He, Q. Chen, and Q. Liu, "Lattice Boltzmann Methods for Multiphase Flow and Phase-Change Heat Transfer," Prog. Energy Combust. Sci. **52**, 62–105 (2016).

(8) PHENIX Collaboration, "Creation of Quark – Gluon Plasma Droplets with Three Distinct Geometries," Nat. Phys. **15**, 214–220 (2019).

(9) F. Liu, G. Ghigliotti, J. J. Feng, and C.-H. Chen, "Self-Propelled Jumping upon Drop Coalescence on Leidenfrost Surfaces," J. Fluid Mech. **752**, 22–38 (2014).

(10) Y. R. Zhang, X. Z. Jiang, Y. R. Chen, and K. H. Luo, "Self-Propelled Jump Regime in Nanoscale Droplet Collisions : A Molecular Dynamics Study 1 Introduction 2 System Construction and Simulation Details," Commun. Comput. Phys. **23**, 1191–1201 (2018).

(11) Y. J. Jiang, A. Umemura, and C. K. Law, "An Experimental Investigation on the Collision Behaviour of Hydrocarbon Droplets," J. Fluid Mech. **234**, 171 (1992).

(12) R. Bardia, Z. Liang, P. Keblinski, and M. F. Trujillo, "Continuum and Molecular-Dynamics Simulation of Nanodroplet Collisions," Phys. Rev. E - Stat. Nonlinear, Soft Matter Phys. **93**, 1–13 (2016).

(13) K. L. Pan, C. K. Law, and B. Zhou, "Experimental and Mechanistic Description of Merging and Bouncing in Head-on Binary Droplet Collision," J. Appl. Phys. **103**, 064901 (2008).

(14) C.-K. Kuan, K.-L. Pan, and W. Shyy, "Study on High-Weber-Number Droplet Collision by a Parallel, Adaptive Interface-Tracking Method," J. Fluid Mech. **759**, 104–133 (2014).

(15) D. Lycett-brown and K. H. Luo, "Improved Forcing Scheme in Pseudopotential Lattice Boltzmann Methods for Multiphase Flow at Arbitrarily High Density Ratios," Phys. Rev. E **91**, 023305 (2015).

(16) S. E. Mousavi Tilehboni, E. Fattahi, H. H. Afrouzi, and M. Farhadi, "Numerical simulation of droplet detachment from solid walls under gravity force using lattice Boltzmann method," J. Mol. Liq. **212**, 544–556(2015).

(17) J. Qian and C. K. Law, "Regimes of Coalescence and Separation in Droplet Collision," J. Fluid Mech. **331**, 59–80 (1997).

(18) K.-L. Pan, P.-C. Chou, and Y.-J. Tseng, "Binary droplet collision at high Weber number," Phys. Rev. E: Stat., Nonlinear, Soft Matter Phys. **80**, 036301 (2009).

(19) P. Zhang and C. K. Law, "An Analysis of Head-on Droplet Collision with Large Deformation in Gaseous Medium," Phys. Fluids **23**, 042102 (2011).

(20) J. Li, "Macroscopic Model for Head-On Binary Droplet Collisions in a Gaseous Medium," Phys. Rev. Lett. **117**, 214502 (2016).

(21) M. H. Taheri, M. Mohammadpourfard, A. K. Sadaghiani, and A. Kosar, "Wettability alterations and magnetic field effects on the nucleation of magnetic nanofluids: A molecular dynamics simulation," J. Mol. Liq. **260**, 209–220 (2018).

(22) F. Taherian, V. Marcon, E. Bonaccurso, and N. F. van der Vegt, "Vortex Formation in Coalescence of Droplets with a Reservoir Using Molecular Dynamics Simulations," J. Colloid Interface Sci. **479**, 189-198 (2016).

(23) Y. R. Zhang and K. H. Luo, "Regimes of Head-On Collisions of Equal-Sized Binary Droplets," Langmuir **35**, 8896–8902 (2019).

(24) Y. R. Zhang, X. Z. Jiang, and K. H. Luo, "Bounce Regime of Droplet Collisions: A Molecular Dynamics Study," J. Comput. Sci. **17**, 457–462 (2016).

(25) L. Zhao and P. Choi, "Molecular Dynamics Simulation of the Coalescence of Nanometer-Sized Water Droplets in n-Heptane," J. Chem. Phys. **120**, 1935 (2004).

(26) M. Svanberg, L. Ming, N. Marković, and J. B. C. Pettersson, "Collision Dynamics of Large Water Clusters," J. Chem. Phys. **108**, 5888 (1998).

(27) D. Sundaram, V. Yang, and R. A. Yetter, "Metal-Based Nanoenergetic Materials: Synthesis, Properties, and Applications," Prog. Energy Combust. Sci. **61**, 293–365 (2017).

(28) V. Molinero and E. B. Moore, "Water Modeled As an Intermediate Element between Carbon and Silicon," J. Phys. Chem. B **113**, 4008–4016 (2009).

(29) H. M. Aktulga, J. C. Fogarty, S. A. Pandit, and A. Y. Grama, "Parallel Reactive Molecular Dynamics : Numerical Methods and Algorithmic Techniques," Parallel Comput. **38**, 245–259 (2012).

(30) W. Humphrey, A. Dalke, and K. Schulten, "VMD: Visual molecular dynamics," J. Mol. Graphics Model. **14**, 33−38 (1996).

(31) A. Stukowski, "Visualization and analysis of atomistic simulation data with OVITO-the Open Visualization Tool," Model. Simul. Mater. Sci. Eng. **18**, 015012 (2010).

(30) S. Wildeman, C. Visser, N. Nikolopoulos, and G. Bergeles, "The Effect of Gas and Liquid Properties and Droplet Size Ratio on the Central Collision between Two Unequal-Size Droplets in the Reflexive Regime," Int. J. Heat Mass Transf. **54**, 678–691 (2011).

(33) N. Nikolopoulos, G. Strotos, K. S. Nikas, and G. Bergeles, "The Effect of Weber Number on the Central Binary Collision Outcome between Unequal-Sized Droplets," Int. J. Heat Mass Transf. **55**, 2137–2150 (2012).

(34) A. L. Yarin, "Drop impact dynamics: Splashing, spreading, receding, bouncing," Annu. Rev. Fluid Mech. **38**, 159−192 (2006).

(35) G. Finotello, J. T. Padding, N. G. Deen, A. Jongsma, F. Innings, and J. A. M. Kuipers, "Effect of Viscosity on Droplet-Droplet Collisional Interaction," Phys. Fluids **29**, 067102 (2017).

(36) M.-L. Liao, S.-P. Ju, and S.-H. Yang, "Coalescence Behavior of Water Nanoclusters : Temperature and Size Effects," J. Phys. Chem. C **111**, 6927–6932 (2007).

(37) J. C. Pothier and L. J. Lewis, "Molecular-Dynamics Study of the Viscous to Inertial Crossover in Nanodroplet Coalescence," Phys. Rev. B - Condens. Matter Mater. Phys. **85**, 1–10 (2012).

(38) Q. C. Chen, J. Ma, H. M. Xu, and Y. J. Zhang, "The impact of the ionic concentration on electrocoalescence of the nanodroplet driven by dielectrophoresis," J. Mol. Liq. **290**, 111214 (2019).

(39) K. Willis and M. Orme, "Binary Droplet Collisions in a Vacuum Environment: An Experimental Investigation of the Role of Viscosity," Exp. Fluids **34**, 28–41 (2003).

(40) S. F. Kharmiani, M. Passandideh-Fard, and H. Niazmand, "Simulation of a single droplet impact onto a thin liquid film using the lattice Boltzmann method," J. Mol. Liq. **222**, 1172–1182 (2016).

(41) K. D. Willis and M. E. Orme, "Experiments on the Dynamics of Droplet Collisions in a Vacuum," Exp. Fluids **29**, 347–358 (2000).

All figure captions

Figure 1. Configuration of droplet collision system.

Figure 2. Snapshots of 10 nm droplet collisions at the Weber number of (a) 277, (b) 426 and (c) 540, respectively.

Figure 3. Snapshots of 50 nm droplet collisions at the Weber number of (a) 277 and (b) 500, respectively.

Figure 4. Kinetic energy evolutions of 50 nm droplet collisions at the Weber number of 277 and 500, respectively.

Figure 5. Snapshots of 100 nm droplet collisions at the Weber number of (a) 200 and (b) 277, respetively.

Figure 6. Kinetic energy evolutions of 100 nm droplet collisions at the Weber number of 200 and 277, respectively.

Figure 7. Cross-section view of reflexive separation regime (D=100 nm, We=277).

Figure 8. Component analysis of parent and child droplets.

Figure 9. Density contours on the cross section of 50 nm droplet collisions at the Weber number of 277.

Figure 10. Maximum stretching factors of the 10, 50 and 100 nm droplets as a function of the Weber number.

Figure 11. Kinetic energy evolutions for the 10, 50 and 100 nm droplets under the Weber number of 277.

Figure 12. Comparison of droplet collision regimes at nanoscale and macroscale.

All tables

Table 1. Values of potential parameters

σ	ε	a	λ	γ	$\cos\theta_0$	A	B	p	q
2.3925	6.189	1.8	23.15	1.2	-0.33	7.0496	0.6022	4.0	0.0

Data Availability Statement

The data that support the findings of this study are available from the corresponding author upon reasonable request.